International Journal of Engineering

Journal Homepage: www.ije.ir

Coded Thermal Wave Imaging Based Defect Detection in Composites using Neural Networks

M. Parvez M.*[a], J. Shanmugam[a], M. Sangeetha[a], V. S. Ghali[b]

[a] *Department of Electronics and Communication Engineering, Bharath Institute of Higher Education and Research, Chennai, TN, India*
[b] *Department of Electronics and Communication Engineering, Koneru Lakshmaiah Education Foundation, Vaddeswaram, AP, India*

PAPER INFO

Paper history:
Received 18 August 2021
Received in revised form 26 September 2021
Accepted 01 October 2021

Keywords:
Active Thermography
Artificial Nueral Network
Bi-phase Coded
Probability of Detection
Signal To Noise Ratio

ABSTRACT

Industry 4.0 focuses on the deployment of artificial intelligence in various fields for automation of variety of industrial applications like aerospace, defence, material manufacturing, etc. Application of these principles to active thermography, facilitates automatic defect detection without human intervention and helps in automation in assessing the integrity and product quality. This paper employs artificial neural network (ANN) based classification post-processing modality for exploring subsurface anomalies with improved resolution and enhanced detectability. A modified bi-phase seven-bit barker coded thermal wave imaging is used to simulate the specimens. Experimentation has been carried over carbon fiber reinforced plastic (CFRP) and glass fiber reinforced plastic (GFRP) specimens using artificially made flat bottom holes of various sizes and depths. A phase based theoretical model also developed for quantitative assessment of depth of the anomaly and experimentally cross verified with a maximum depth error of 3%. Additionally, subsurface anomalies are compared based on probability of detection (POD) and signal to noise ratio (SNR). ANN provides better visualization of defects with 96% probability of detection even for small aspect ratio in contrast to conventional post processing modalities.

doi: *10.5829/ije.2022.35.01a.08*

1. INTRODUCTION

There is a growing demand for applications in load-bearing structures such as transportation instruments, aerospace equipment, wind turbines, and medical devices. Therefore, to minimize the essential security concerns and maintenance cost, a robust and consistent non-destructive testing (NDT) is necessary for testing of composite materials [1]. In general, NDT consists of various non-invasive inspection techniques [2-3] to assess the material properties and structural characteristics of the components, or entire processing units. The demand for material defect detection increases various challenges in NDT [4-6]. Compared to traditional NDT methods, infrared thermography is a new NDT technology that has evolved rapidly in the recent years.

Active infrared thermography grabs the attention as a reason of fast, complete field, non-invasive and non-contact defect detection characteristics. Several categories of active infrared thermography, based on the input stimulus are pulse thermography (PT), pulse phased thermography (PPT), lock-in thermography (LT), and Non-Stationary Thermal Wave Imaging (NSTWI). Pulse thermography uses an external heat stimulus of high power for a small duration to energize the test specimen [7]. The requirement in extreme power and effects associated to non-uniform are significant limitations for the case of pulse thermography. Subsequently, to surmount constraints of pulse thermography with a continuous sinusoidal input stimulus of low power, the lock-in thermography is introduced. In pulse phased thermography phase based analysis is performed to explore the subsurface details. The investigation is similar to pulse thermography, in pulse phased thermography a phase-based analysis is performed as like lock-in thermography [8-9]. Since the sinusoidal stimulus consists of mono frequency, it can probe into a particular depth only. However, in realistic

*Corresponding Author Institutional Email: parvez@kluniversity.in (M. Parvez M.)

Please cite this article as: M. Parvez M., J. Shanmugam, M. Sangeetha, V. S. Ghali, Coded Thermal Wave Imaging Based Defect Detection in Composites using Neural Networks, ***International Journal of Engineering, Transactions A: Basics***, Vol. 35, No. 01, (2022) 93-101

scenario anomalies may occur at different locations. To test the realistic scenarios, it is required to perform repetitive experiments with altered frequencies which is a major constraint for its applicability [10]. Moreover, the requirement of high power is the major drawback of pulse phased thermography [11].

However, to examine an object in single experimentation for a small duration of time, non-stationary thermal wave imaging is used [12]. Linear frequency modulated thermography uses frequency modulated chirp stimulus of low power through lower frequency band towards the test of entire sample during a particular investigation. Since the low frequency probes deep into the object, it explores the subsurface characteristics [13]. Later, quadratic frequency modulated thermography uses quadratic chirp. The quadratic chirp signal probes more deeply into the object than its linear counterpart, and it gives the visualization, in-depth details with better contrast [14].

In recent years, an evolving non-stationary thermal wave imaging system with its unique depth resolution and defect detection characteristics is Barker coded thermal wave imaging (BCTWI). The present work uses BCTWI followed by artificial neural network (ANN) based on post-processing technique to explore the subsurface details. Employing various signal processing algorithms, the processing of recorded thermal response is handled to obtain the qualitative and quantitative subsurface details. The obtained results are compared with the metrics via full width at half maxima (FWHM), probability of detection (POD), and signal to noise ratio (SNR).

Barker coded thermal wave imaging system is implemented in this work to facilitate high depth resolution and sensitivity, by suppressing the limited resolution and by increasing the depth probing capabilities. It was found that detection performance and depth resolution can be enhanced by decrease in the size of side lobes than main lobe due to concentration of greater energy. This can be achieved through the system of barker coded thermal wave imaging. In brief, for detecting the defects and estimating its relative sizes, the neural network basis classification framework was implemented. Furthermore, by the way of backscatter signals from the concept of BCTWI the quantitative depth estimation has been carried out. ANN based analysis is ensured to have experimentally enhanced reliability, defect detection of artificially created bottom holes in the materials of GFRP and CFRP, quantitative estimation of depths using BCTWI.

Organization of manuscript is as follows: section I introduces thermography with the necessity for barker coded thermal wave imaging and section 2 provides theory of barker coded thermal wave imaging technique followed by experimentation and processing techniques in section 3. Later, section 4 discusses a brief note about the results.

2. CONCEPT OF THERMAL BARKER CODED THERMAL WAVES

A model associated with thermal wave propagation based on heat equations involves the backscatter of the waves for evaluating the subsurface anomalies and validation as well. In BCTWI a code-based stimulus is emitted near to test object surface that relatively provokes thermal waves close to the surface propagating into the interiors of the object [15, 16]. Resulting thermal waves that are propagated signifies towards the back as of the boundary leading to temperature rise above object surface. Also, the response of temperature is quantified in resolving a 1D heat equation assuming coordinate system to be rectangular and is shown in Equation (1).

$$\frac{\partial^2 T}{\partial x^2} = \frac{1}{\alpha}\frac{\partial T}{\partial t} \tag{1}$$

Here diffusion coefficient is symbolized as ‘α’, T (x, t) denotes instant temperature at a given time instance ‘t’ with equivalent value of depth as ‘x’, coded flux having peak power is signified as Q_0. With the consideration of delayed step responses in combination, the excited stimulation is given as in Equation (2).

$$Q(t) = Q_0 \sum_{i=1}^{4} (-1)^{n_i}\, u\left(t - a_i \tau\right) \tag{2}$$

where n_i=0,1,2,3 and a_i =0,3,5,6

Under the adiabatic boundary condition, the equation for heat diffusion is solved, i.e., exchange of heat flux by backward portion stands at insignificant rate, as followed in Equation (3).

$$-k \left.\frac{\partial T}{\partial x}\right|_{x=L} = 0 \tag{3}$$

The test object surface is stimulated using BCTWI. Over the surface sample, the obtained incident energy will be attenuated in a thin layer, further a related heat flux is produced on the sample upper surface as in Equation (4).

$$-k \left.\frac{\partial T}{\partial x}\right|_{x=0} = \sum_{i=1}^{4} (-1)^{n_i}\, u\left(t - a_i \tau\right) \tag{4}$$

where ‘k’ indicates thermal conductivity of material, presumed not a dependable quantity of temperature and finite thickness of the sample is denoted with ‘L’. By

solving Equation (1) with the above conditions, the specimen's thermal response is obtained in the Laplacian domain is shown by Equation (5).

$$T(x,s)=\frac{Q(s)e^{-\sigma x}}{k\sigma} \tag{5}$$

The corresponding radiation of the received thermal response with the help of an IR sensor with a sampling rate of 'fs' is captured. Further, it can be determined by using the following equations.

$$R(x,w)=\mu_r\int_0^d T(x,w)e^{-\mu x}dx$$

$$R(\mathrm{d},w)=\frac{-\mu_r\sqrt{\alpha}Q(jw)}{k\sqrt{jw}}\left(\frac{1}{\left(\sqrt{\frac{jw}{\alpha}}+\mu\right)}-\frac{e^{\left(\sqrt{\frac{w}{2\alpha}}+\mu\right)d}e^{j\sqrt{\frac{w}{2\alpha}}d}}{\left(\sqrt{\frac{jw}{\alpha}}+\mu\right)}\right)$$

where 'μ_r' is infrared absorption coefficient and $Q(jw)=\frac{1}{jw}\left[1-e^{-3jw}-e^{-5jw}-e^{-6jw}\right]$

$$R(d,w)=\frac{\mu\sqrt{\alpha}\left[1-e^{-3jw}-e^{-5jw}-e^{-6jw}\right]}{kjw\sqrt{jw}}\left(\frac{1-e^{-\left(\sqrt{\frac{jw}{\alpha}}+\mu\right)d}}{\left(\sqrt{\frac{jw}{\alpha}}+\mu\right)}\right) \tag{6}$$

Put $jw=\frac{\log\left(re^{j\theta}\right)}{t}$ and extract the phase component in Equation (6),

$$\phi_{CZT}=\frac{\pi}{4}-\frac{\theta}{2t}-\sqrt{\frac{\theta}{2t\alpha}}d-\phi_1+\tan^{-1}\left(-\frac{\sqrt{\frac{\theta}{2t\alpha}}}{\mu_a+\frac{1}{\sqrt{2t\alpha}}}\right) \tag{7}$$

$$\phi_1=\tan^{-1}\left(\frac{\sin\left(\frac{7\theta}{2t}\right)\sin\left(\frac{\theta}{2t}\right)+\sin\left(\frac{3\theta}{2t}\right)\sin\left(\frac{\theta}{2t}\right)}{\cos\left(\frac{7\theta}{2t}\right)\cos\left(\frac{\theta}{2t}\right)+\cos\left(\frac{3\theta}{2t}\right)\cos\left(\frac{\theta}{2t}\right)}\right)$$

From Equation (7), the extracted phase proportionally changes with respect to depth associated with defect, which is further applied to estimate the depth of defects.

3. EXPERIMENTATION AND PROCESSING

The active thermal wave imaging scheme illustration is depicted through Figure 1. In present experimental setup, the sample is kept opposite to a pair of halogen lights, which are of 1KW power each. The sample is stimulated by an optical stimulus with a sweep frequency rate of 0.01-0.1Hz for duration of 100 s with 25Hz frame rate. However, Infrared (IR) camera is positioned at one meter opposite to test sample, to record the reflected thermal response. The halogen lamps were placed to facilitate a uniform illumination. The 7-bit barker-coded optical stimulus is enacted uniformly on the surface of test sample, then its corresponding temperature contrast over the test sample will be captured by IR camera [15]. Initially, the captured thermal response is processed by using a suitable linear fitting procedure to remove the static response and to retain the dynamic part of the response. The dynamic part of captured thermal response will undergo further post processing using suitable signal processing techniques and ANN based algorithm to analyze the subsurface features.

3. 1. Pre-processing To minimize the non-uniformity in the emission, the radiation issues and to visualize the subsurface anomalies accurately, signal processing algorithms are employed over the dynamic part of the recorded response. With the help of appropriate linear fitting technique on the recorded infrared data, the dynamic part is retained by eradicating of static part from the response.

3. 2. Post-processing

3. 2. 1. FFT Phase For separation of frequency, the FFT phase employs a fast Fourier transform (FFT). In the current investigation, over the thermal profile at each pixel value the FFT is employed [17]. At each frequency component the phase values are determined, thereby assigning corresponding phase values of frequency components to the respective pixel positions in a systematic manner for developing the phase grams. Moreover, the phase image constructed exhibits contrast phase because of the phase delay associated from anomalies of thermal waves at various depths [18]. Accordingly, the frequency consistent to the phase image demonstrating the determination of defects as stated in Equation (8).

$$f=\frac{F_S n}{N} \tag{8}$$

where Fs is rate of capture or sampling frequency, n is

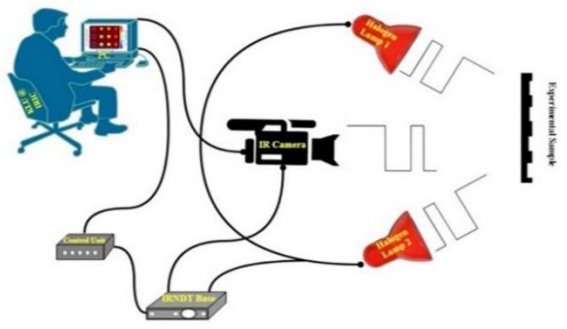

Figure 1. Pictorial Representation of the active thermal wave imaging scheme

quantity of the phase image, and N is quantity of the samples in thermal profile.

3. 2. 2. Hilbert Phase In this method a time domain phase is used to discriminate the defective locations from its counter parts. In the first stage, Hilbert transform based pulse compression is performed by using Equation (9). In the next stage, the ordinary pulse compression value is determined using Equation (10). Further, the time-domain phase of a particular pixel is obtained by using Equation (11) [19].

$$Q_1 = IFFT\left[\left\{FFT\left(Hilb\left(T_r\right)\right)\right\} * \left\{FFT\left(T\right)\right\}\right] \quad (9)$$

Furthermore, in the next phase procedure, the normal cross-correlation can be performed among the thermal profile as reference and temporal for individual pixels as shown in Equation (10).

$$Q_2 = IFFT\left[\left\{FFT\left(T_r\right)\right\} * \left\{FFT\left(T\right)\right\}\right] \quad (10)$$

Finally, the time domain phase will be obtained using

$$\theta = \tan^{-1}\left(\frac{Q_1}{Q_2}\right) \quad (11)$$

by re-arranging the outcome phase values into corresponding positions, the time-domain phase images are obtained.

3. 2. 3. Pulse Compression As per the methodology, the attenuation and delay possessed through correlated thermal waves are used to discriminate the defective locations from its counterparts [20]. Initially during the period of stage 1, a thermal profile as a reference point is carefully chosen as of the exact location of the region that is non-defective. Later, with the help of reference point the interrelationship for the two points said to be the cross-correlation is conducted, which results a correlation coefficient sequence between 0 to 1 using Equation (12). These obtained normalized correlation coefficients are rearranged into their corresponding pixel locations to form correlation images for that delayed instant. The correlation contrast in constructed images is helpful to visualize the defects. This coefficient contrast obtained can be utilized for subsurface feature extraction [21].

$$g\left(\tau\right) = \int_{-\infty}^{\infty} s\left(t\right) h\left(\tau + t\right) dt \quad (12)$$

Figure 2 shows the block diagram representation of various signal processing methods [21]. Figures 2a and 2b show the processing approaches steps for obtaining the frequency domain-based results whereas Figure 2c shows the processing steps to obtain time-domain phase results.

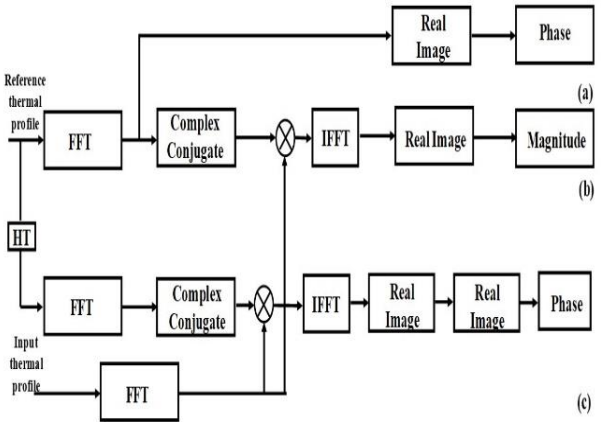

Figure 2. Block diagram representation of various singnal processing approaches

3. 2. 4. Artificial Neural Network Based on the research undertaken in the area of Inverse Heat Transfer Problem (IHTP), this study aims for quantitative and qualitative detection of defects through ANN based model, which is further validated experimentally [22].

The Artificial Neural Networks (ANN) have been widely used to classify the information regarding subsurface characteristics qualitatively and quantitatively. This contribution focuses on qualitatively assessing the subsurface anomalies using classification-based modality using ANN and quantitatively visualizing the depth of anomalies using phase-based depth assessment using BCTWI. Generally, ANNs comprise of units that are interconnected which are termed as artificial neurons as depicted in Figure 3. Input layer (Input) is considered as temporal thermal profile information and associated parameters (neurons) offer over the output (output layer), correspondingly the other neurons from the view are hidden (hidden layers). Based on the interconnection between neurons, the network membership function is determined, in which the connections are not simple, merely particular non-linear functions [23-25]. The network utilizes multilayer perceptron NN using 250 input nodes. The network employs successive hidden layers which has nodes about 50 and 25, respectively. These nodes were used for training and analysis partitioning as two targets carrying single output node which is signified as targeted areas of defective and non-defective regions. For detection and quantification assessment, a tan-sigmoid activation function is utilized in combination with the back propagation neural network (BPNN). Through the classification based supervised learning, the detection and quantification of irregularity characteristics including depth and location is conducted in the range of two successive actions. The temporal

sequence of the thermograms is first recorded, later training vectors are formed correspondingly to the data acquisition. In a sequence, input count is equivalent to the thermogram count using which training vectors are formed. After the adjustment of weights through back propagation, the outputs offered are defected and non-defected region.

3. 2. 4. 1. Clasiification Mode for Anomaly Detection To model and detect the features of subsurface of inverse thermography problem, the classification employs the phases of training and testing phase. The temporal thermal response of defect spots resembles the unique characteristics of subsurface anomalies in the terms of delay and attenuation, but non-defective points retain similar properties that employs in classifying defect points for particular methodology. In the phase of training, the removal of mean thermal profile at some defect-free spots (100 intended for the case) were down sampled further utilized for network training. In which the network has achieved 100 times targeting "0" over such period of 150 s with the system configuration of Intel 7 processor with specifications of 16 GB RAM, 512 GB SSD.

For recognition, the data provided during the test phase should be classified into defective and non-defective points. Each down converted pixel in the case of temporal thermal can be given as input i.e., input layer, then propagates additional to the hidden layer besides eventually stretched to the output layer, which produces whichever a defective or a non-defective class. It uses a backpropagation algorithm to set weights and generate binary values based on the state of the output. The Backpropagation (BP) algorithm uses the method of gradient descent to seek the minimum of the error function by optimal weight nodes [17]. Consider a Neural Network (NN) with k inputs and l outputs, in which, w_{ij} is the weight associated with the interconnection between the node of one layer and the node of the next layer. Besides, are denoted by the input and target of the dataset respectively; is the outputs of neural networks with the inputs. The minimized error function of the network is described as Equation (13).

$$E = \frac{1}{n}\sum_{i=1}^{n}\left\|o_i - y_i\right\|^2 \tag{13}$$

The BPNN aims to look for a local point that represents a minimum of the error function. The initial weights are selected stochastically by the BP algorithm. In the next stage, to correct initial weight, using an iterative process of gradient descent, the error function computes repeatedly [23] using Equation (14).

$$\nabla E = \frac{\partial E1}{\partial w_{ij}} \tag{14}$$

Each weight is updated with the following Equation (15).

$$\nabla w_{ij} = -\gamma \frac{\partial E}{\partial w_{ij}} \tag{15}$$

The weight's updating of BPNN can be obtained by using Equation (16).

$$w_{ij}(t+1) = w_{ij}(t) + \Delta w_{ij}(t)$$
$$w_{ij}(t+1) = w_{ij}(t) - \gamma \frac{\partial E}{\partial w_{ij}} + \xi(t) \tag{16}$$

where, γ is the constant or learning rate of NN, and $\xi(t)$ is a stochastic term. Defective areas can be characterized with "1" and non-defective areas can be characterized by "0". Consequently, with the detection outcome, all pixels exist under thermogram can be further categorized as non-defective or defective areas of the test sample [22-23].

3. 2. 4. 2. Estimation of Depth In order to estimate and visualize the depths quantitatively, Fast Fourier transform is applied over each and every thermal profile pertaining to each pixel location in view and corresponding phase images were developed. Chirp z transform is applied over selected range of frequencies [26] about the frequency corresponding to the best phase image possessing all the subsurface details. Further, this phase value is converted to the corresponding depth value using Equation (7) and phase value of each pixel in view is represented with this corresponding value quantitatively in Figure 10; thus, the subsurface features will be represented in terms of their corresponding depths for ease of further analysis.

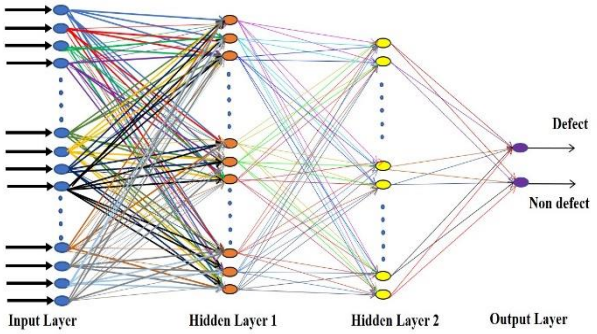

Figure 3. Block diagram of neural network used for classification of defects

4. RESULTS AND DISCUSSIONS

With the two samples of Glass fiber reinforced plastic (GFRP) and Carbon fiber reinforced plastic (CFRP), the experimentation has been undertaken to assess the proposed approach. The GFRP sample consists of 10 Teflon patches with different size variations at two different depth value. Whereas the CFRP sample comprises of 12 artificially made flat bottom holes with size variations at variety of depth rates as depicted in Figure 4.

By means of 7-bit barker coded optical stimulus, the sample to be tested has been energized for a time period of 100s. The pair of halogen lamps, which are of 1 kW power each one is focused on the test sample. With the help of camera that is maintained at 1m distance to the test sample holding specifics of FLIR SC 655A IR with spectral range of 7.5-14µm and 25 fps, the temporal thermal response has been captured from the surface region of test sample. Figure 5 depicts the set up for experimentation for active infrared thermography.

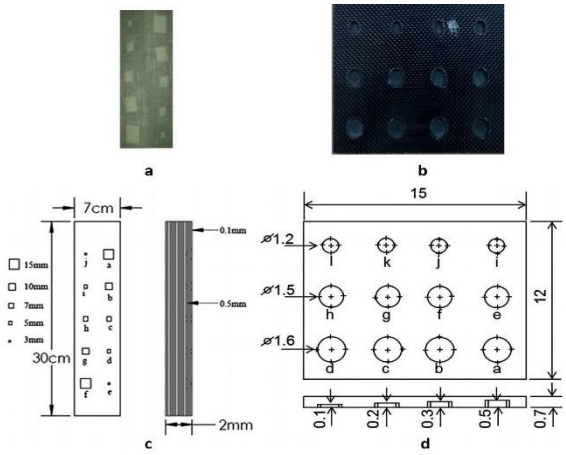

Figure 4. Experimental a. GFRP and b. CFRP specimen & Layout of c. GFRP and d. CFRP specimen

Figure 5. Active infrared tehrmography experimental setup

To obtain subsurface features using a suitable post-processing method, the mean from thermal profiles is removed to extract the dynamic response of each pixel. In comparison with conventional methods for processing such as PC, FFT phase, Hilbert phase and ANN based method is also implemented against detrended (detached mean) contour profile for extracting the details of subsurface. Figure 6 represents the processed results to visualize the subsurface details by using different post processing methods and proposed ANN method for experimental specimen of GFRP. Figure 7 illustrates the subsurface details of CFRP sample by means of different post processing methods and proposed ANN methodology.

Figures 6d and 7d show the artificial neural network-based classification modality exhibits all the defects with good contrast and better visualization. Among several processing approaches, the artificial neural network offers superior detectability with good contrast.

Eventually, the detectability of several processing methods can be measured by the help of signal to noise ratios (SNR). The calculation of SNR of individual pixel is done by means Equation (17) for which the mean of the defective and non-defective area along with standard deviation of the non-defective region are

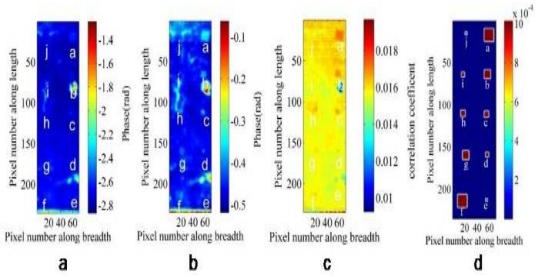

Figure 6. Outputs of a. FFT Phase b. Hilbert phase c. Pulse compression d. Aritificial neural networks for GFRP sample

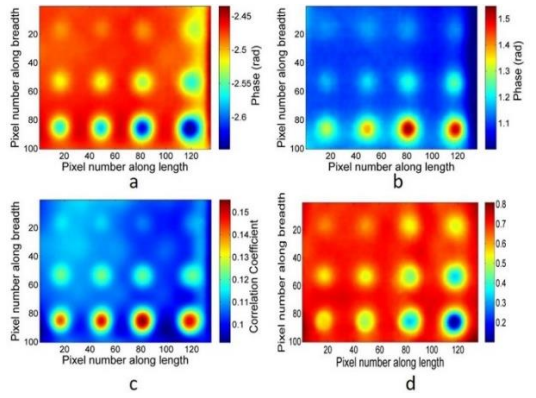

Figure 7. Outputs of a. FFT Phase b. Hilbert phase c. Pulse compression d. Aritificial neural networks for GFRP sample

calculated [27]. The SNR's of CFRP and GFRP samples for various processing methods and proposed ANN method is represented in Figures 8 and 9, respectively. It is clear from the Figures 8 and 9; the artificial neural network-based methodology provides us better results compared to that of other processing methodologies.

$$SNR(dB)=\frac{\text{mean of defective area-mean of non defective area}}{\text{standard deviation of non defective area}} \quad (17)$$

4. 1. Analysis for Quantitative Depth FFT is applied over thermal profile and corresponding phase images were generated among them phase gram at 0.01hz is presenting all the subsurface details hence, the frequency band 0.005-0.015hz is zoomed with 8192 samples and observing corresponding phase values the phase gram at 0.01056hz is presented the defects very clearly. Hence corresponding phase values of the defects were taken for quantification leading to the depth estimation as shown in Figure10 of CFRP.

4. 2. Defect Sizing The full width at half maxima (FWHM) method has utilized for calculation of defect sizing [27]. The sizing of defects at different depths of the GFRP sample for different processing methods has been computed, and the obtained values are shown in Table 1. The size estimated from the artificial neural network nearly resembles that of the actual defect size.

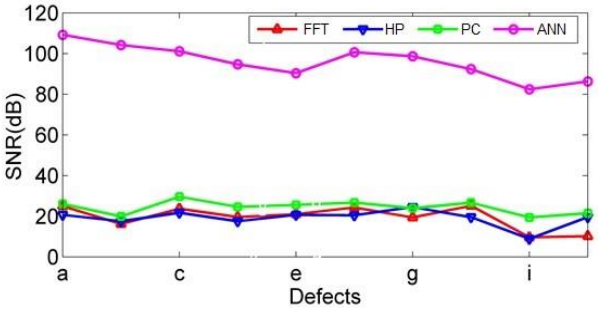

Figure 8. SNR for processed results of GFRP data

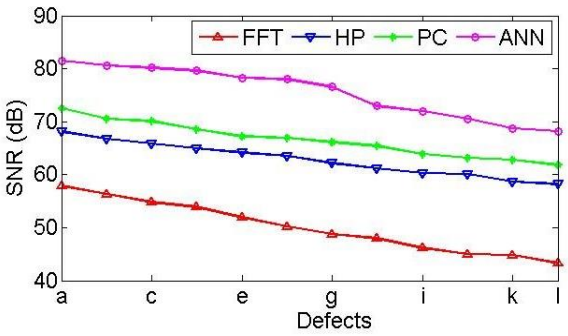

Figure 9. SNR for processed results of CFRP data

4. 3. Probability of Detection (POD) As per the industrial requirements processing method mush possess the high reliability in terms of defect detection even for small aspect ratios, reliability of the proposed modality is evaluated through POD [27-28].

Figure 11 depicts about the estimate of POD as well as aspect ratio of a variety of post-processing techniques such as artificial neural networks (ANN), pulse compression (PC), Hilbert phase (HP), and phase analysis (FFT). From the above figure, the ANN has the highest Probability of detection even for small aspect ratios as compared to the other post-processing methodologies.

TABLE 1. Comparison of processed data for full width half maxima

Sample	Defect	Actual Size (mm)	FFT Phase	HP	PC	ANN
	a	15	14.11	14.22	14.32	**15.12**
	b	10	9.21	9.13	9.7	**10.12**
GFRP	c	7	6.12	7.62	6.48	**7.01**
	d	5	4.63	4.31	4.82	**5.11**
	e	3	2.68	2.64	2.83	**3.03**

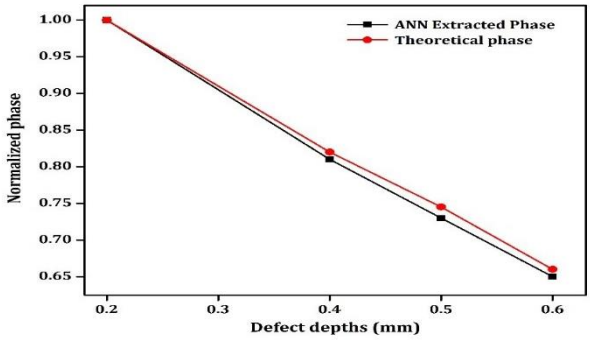

Figure 10. Defects involved for CFRP samples in respective to depth verses phase constrast

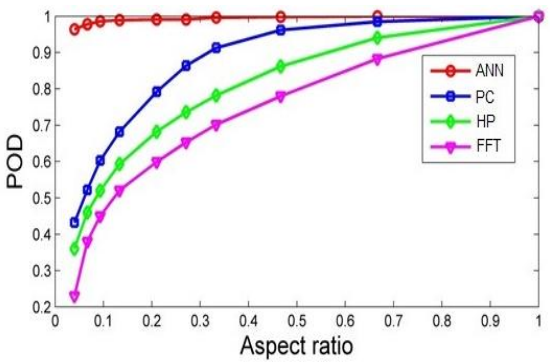

Figure 11. Curve of POD for various post-processing methods

5. CONCLUSION

To detect and differentiate subsurface anomalies in the experimentation of GFRP and CFRP specimens, the artificial neural network-based classification technique is employed using BCTWI. By exerting the experimental validation, the capability of the proposed ANN-based approach has been demonstrated. A phase based theoretical model was developed with a maximum depth error of 3%. The obtained results evident for the estimation of sizing by applying full width at half maxima with an average error percentage of 4.2 including the reliability at the combined analysis of POD based assessment. SNR is also considered to further validate the potentiality of detecting the defects. Based on the above validation parameters the analysis dependent on ANN technique holds by experimentation is achieved with enhanced reliability, detection of depth and evaluation of the subsurface anomalies quantitatively by employing BCTWI.

6. REFERENCES

1. X. Maldague, Theory and practice of infrared thermography for non-destructive testing. New York, US: Wiley, 2001.
2. J. González-Durán, M. Zamora-Antuñano, L. Lira-Cortés, J. Rodríguez-Reséndiz, J. Olivares-Ramírez and N. Lozano, "Numerical Simulation for the Combustion Chamber of a Reference Calorimeter", ***Processes***, Vol. 8, No. 5, (2020), 575. doi: 10.3390/pr8050575.
3. J. González-Durán, J. Rodríguez-Reséndiz, J. Ramirez, M. Zamora-Antuñano and L. Lira-Cortes, "Finite-Element Simulation for Thermal Modeling of a Cell in an Adiabatic Calorimeter", ***Energies***, Vol. 13, No. 9, (2020), 2300, doi: 10.3390/en13092300.
4. T. Yektaniroumand, M. Niaz Azari and M. Gholami, "Optimal Rotor Fault Detection in Induction Motor Using Particle-Swarm Optimization Optimized Neural Network", ***International Journal of Engineering, Transactions B: Applications***, Vol. 31, No. 11, (2018), 1876-1882. doi: 10.5829/ije.2018.31.11b.11.
5. H. Bui et al., "Characterization of Electrical Conductivity of Anisotropic CFRP Materials by Means of Induction Thermography Technique", ***IEEE Transactions on Magnetics***, Vol. 54, No. 3, (2018), 1-4, doi: 10.1109/tmag.2017.2742979.
6. H. Kim, "FPGA-based of Thermogram Enhancement Algorithm for Non-destructive Thermal Characterization", ***International Journal of Engineering, Transactions A: Basics***, Vol. 31, No. 10, (2018), 1675-1681, doi:10.5829/ije.2018.31.10a.09.
7. X. Guo and V. Vavilov, "Pulsed thermographic evaluation of disbonds in the insulation of solid rocket motors made of elastomers", ***Polymer Testing***, Vol. 45, (2015), 31-40, doi: 10.1016/j.polymertesting.2015.04.015
8. H. Song, H. Lim, S. Lee, H. Sohn, W. Yun and E. Song, "Automated detection and quantification of hidden voids in triplex bonding layers using active lock-in thermography***", NDT & E International***, Vol. 74, (2015), 94-105, doi 10.1016/j.ndteint.2015.05.004
9. C. Wallbrink, S. Wade and R. Jones, "The effect of size on the quantitative estimation of defect depth in steel structures using lock-in thermography", ***Journal of Applied Physics***, Vol. 101, (2007). doi: 10, 104907, 2007.
10. C. Ibarra Castanedo, N. Avdelidis and X. Maldague, "Qualitative and quantitative assessment of steel plates using pulsed phase thermography", ***Materials Evaluation***, Vol. 63, No. 11, (2005), 1128-1133, doi: 10.1117/12.602360
11. X. Maldague and S. Marinetti, "Pulse phase infrared thermography", ***Journal of Applied Physics*** 79, No. 5, (1996), 2694-2698, doi: 10.1063/1.362662.
12. G. Dua, V. Arora and R. Mulaveesala, "Defect Detection Capabilities of Pulse Compression Based Infrared Non-Destructive Testing and Evaluation", ***IEEE Sensors Journal***, Vol. 21, No. 6, (2021), 7940-7947. doi: 10.1109/jsen.2020.3046320.
13. J. Ahmad, A. Akula, R. Mulaveesala, and H. K. Sardana, "Barker coded thermal wave imaging for non-destructive testing and evaluation of steel material", ***IEEE Sensors Journal***., Vol. 19, No. 2, (2019), 735-742. doi: 10.1109/JSEN.2018.2877726
14. G. Chandra Sekhar Yadav, V. Ghali and N. Baloji, "A Time Frequency-Based Approach for Defect Detection in Composites Using Nonstationary Thermal Wave Imaging", ***Russian Journal of Non-destructive Testing***, Vol. 57, No. 6, 486-499, (2021). doi: 10.1134/s1061830921060061.
15. M. Parvez M, J. Shanmugam and V. Ghali, "Decision tree-based subsurface analysis using Barker coded thermal wave imaging", ***Infrared Physics & Technology***, Vol. 109, (2020), 103380. doi: 10.1016/j.infrared.2020.103380.
16. M. Parvez, J. Shanmugam and V. Ghali, "Fuzzy C-based Automatic Defect Detection using Barker Coded Thermal Wave Imaging", ***International Journal of Performability Engineering***, Vol. 17, No. 5, (2021), 484. doi: 10.23940/ijpe.21.05. 8.484490.
17. M. Mahani and M. Besanjideh, "Nonlinear and Non-stationary Vibration Analysis for Mechanical Fault Detection Using EMD-FFT Method", ***International Journal of Engineering, Transactions C: Aspecls***, Vol. 25, No. 4, (2012), 363-372, doi: 10.5829/idosi.ije.2012.25.04c.11.
18. N. Tabatabaei and A. Mandelis, "Thermal-wave radar: a novel subsurface imaging modality with extended depth-resolution dynamic range", ***The Review of Scientific Instruments***, 80 (2009) 034902. doi: 10.1063/1.3095560
19. J. A. Siddiqui, S. Patil, S. S. Chouhan, S. Wuriti, V. Arora, and R. Mulaveesala, "An efficient pulse compression favourable thermal excitation scheme for non-destructive testing using infrared thermography", ***Electron Letters***, Vol. 56, No. 19, 1003-1005, (2020). doi: 10.1049/el.2020.0914
20. A. Vijaya Lakshmi, V. Gopitilak, M. Parvez, S. Subhani and V. Ghali, "Artificial neural networks based quantitative evaluation of subsurface anomalies in quadratic frequency modulated thermal wave imaging", ***Infrared Physics & Technology***, Vol. 97, (2019), 108-115, doi: 10.1016/j.infrared.2018.12.013.
21. N.Saeed, M. A.Omar, Y.A.Rahman, "A neural network approach for quantifying defects depth, for non-destructive testing thermograms", ***Infrared Physics & Technology*** 94 (2018), 55-64, doi: 10.1016/j.infrared.2018.08.022
22. S. Dudzik, "Investigations of a heat exchanger using infrared thermography and artificial neural networks", ***Sensors and Actuators A: Physical,*** Vol. 166, No. 1, (2011), 149-156. doi: 10.1016/j.sna.2010.12.001
23. O. Rodriguez-Abreo, J. Rodriguez-Resendiz, C. Fuentes-Silva, R. Hernandez-Alvarado and M. Falcon "Self-Tuning Neural Network PID With Dynamic Response Control***", IEEE Access***, Vol. 9, (2021), 65206-65215, doi: 10.1109/access.2021.3075452.

24. E. Cruz-Miguel, J. García-Martínez, J. Rodríguez-Reséndiz and R. Carrillo-Serrano, "A New Methodology for a Retrofitted Self-tuned Controller with Open-Source FPGA", ***Sensors***, Vol. 20, No. 21, (2020), 6155. doi: 10.3390/s20216155.

25. D. Siddharth, D. K. J. Saini, P. Singh"An Efficient Approach for Edge Detection Technique Using Kalman Filter with Artificial Neural Network", ***International Journal of Engineering, Transactions C: Aspects***, Vol. 34, No. 12, (2021), 1-7, doi: 10.5829/IJE.2021.34.12C.04

26. V. Arora, J.A. Siddiqui, R. Mulaveesala, A. Muniyappa, "Pulse compression approach to non-stationary infrared thermal wave imaging for non-destructive testing of carbon fibre reinforced polymers", ***IEEE Sensors Journal***, Vol. 15, No. 2, (2015), 663-664. doi: 10.1109/JSEN.2014.2361391

27. M. F. Beemer and S. M. Shepard, "Aspect ratio considerations for flat bottom hole defects in active thermography", ***Quantitative InfraRed Thermography***, Vol. 15, No. 1, (2018), 1-16. doi: 10.1080/17686733.2017.1328642

28. M. Keller, Popelin, A. L. Bousquet, N. Bousquet, E. Remy "Nonparametric estimation of the probability of detection of flaws in an industrial component, from destructive and non-destructive testing data, using approximate Bayesian computation", ***Risk Analysis***, Vol. 35, (2015), 1595-1610. doi: 10.1111/risa.12484

Persian Abstract

چکیده

صنعت ۴.۰ بر استقرار هوش مصنوعی در زمینه های مختلف برای اتوماسیون انواع کاربردهای صنعتی مانند هوافضا ، دفاع ، تولید مواد و غیره تمرکز دارد. کاربرد این اصول در ترموگرافی فعال ، تشخیص خودکار نقص را بدون دخالت انسان تسهیل می کند و در ارزیابی. یکپارچگی و کیفیت اتوماسیون کمک می کند محصول این مقاله از روش طبقه بندی مبتنی بر شبکه عصبی مصنوعی (ANN) برای بررسی ناهنجاری های زیر سطحی با وضوح بهتر و قابلیت تشخیص بیشتر استفاده می کند. برای شبیه سازی نمونه ها از یک تصویربرداری موج حرارتی هفت مرحله ای اصلاح شده با پارکر استفاده می شود. آزمایش بر روی نمونه های پلاستیکی تقویت شده با الیاف کربن (CFRP)و پلاستیک تقویت شده با الیاف شیشه (GFRP)با استفاده از سوراخ های ته صاف مصنوعی در اندازه ها و اعماق مختلف انجام شده است. یک مدل نظری مبتنی بر فاز نیز برای ارزیابی کمی عمق ناهنجاری توسعه یافته و به صورت تجربی با حداکثر خطای عمق ۳ cross تأیید شده است. علاوه بر این ، ناهنجاری های زیر سطحی بر اساس احتمال تشخیص (POD)و نسبت سیگنال به نویز (SNR) مقایسه می شوند. ANN تجسم بهتری از نقایص با ۹۶٪ احتمال تشخیص حتی در نسبت ابعاد کوچک در مقایسه با روشهای معمول پردازش پست فراهم می کند.